





Cite this: *Dalton Trans.*, 2018, **47**, 9164

Bipyrrolidine salan alkoxide complexes of lanthanides: synthesis, characterisation, activity in the polymerisation of lactide and mechanistic investigation by DOSY NMR†

James Beament,^a Gabriele Kociok-Köhn,^b Matthew D. Jones ^{*a} and Antoine Buchard ^{*a}

Four dimeric lanthanide alkoxide complexes bearing ONNO bipyrrolidine salan ligands ($L^{\text{Me}}\text{H}_2/L^{\text{tBu}}\text{H}_2$) have been prepared with Nd, Sm and Yb. Depending on the metal and substituents, these complexes adopt varying coordination geometries. While investigating the hydrolytic degradation of these complexes, three dimeric mixed alkoxide/hydroxide and bis-hydroxide products were also prepared, isolated and characterised. Despite paramagnetism, ^1H NMR and diffusion ordered spectroscopy (DOSY) allowed additional characterisation alongside elemental and single-crystal X-ray diffraction analyses. These systems were very active for the controlled ring-opening polymerisation (ROP) of *rac*-lactide (LA), under industrially relevant melt conditions and in solution, yielding complete conversion within 5 minutes at $[\text{Ln}]:[\text{LA}]$ ratios of up to 3000:1 in toluene, and at 80 °C, whilst retaining low dispersities ($D = 1.1$). ^1H DOSY NMR spectroscopy was employed to monitor polymer growth from the metal centres *in situ*, and revealed a dinuclear catalytically active species.

Received 23rd May 2018,
Accepted 18th June 2018

DOI: 10.1039/c8dt02108b
rsc.li/dalton

Introduction

With the dependence on fossil fuel resources and the environmental persistence of most commodity polymers, our societal reliance on plastics is now unanimously viewed as unsustainable.¹ Supported by public opinion, this has triggered a concerted research effort between academia and industry towards the development of sustainable alternatives from renewable resources.^{2–5} Polylactide (PLA), a thermoplastic aliphatic polyester derived from lactic acid, is arguably one of the most widely studied degradable and renewable polymers. PLA is commercially available for packaging and fibre applications,⁶ and prepared through a solvent-free ring-opening polymerisation (ROP) of lactide (LA). LA can be utilised as either the enantiomerically pure *L*-LA, or as a racemic mixture of *D* and *L* monomers (*rac*-LA), the latter allowing atactic, heterotactic or

isotactic microstructures. This is important as the physical properties of the polymer are intrinsically linked to the polymer microstructure, with atactic and heterotactic PLA being amorphous, and heterotactic PLA having a slightly lower T_g (~50 vs. 45 °C).^{7,8} Isotactic PLA is the most sought after structure as it can form a crystalline stereocomplex with a melting temperature ($T_m = 230$ °C) enhanced compared to individual crystalline PLLA or PDLA ($T_m = 180$ °C).⁸ Over the past decades, the drive to achieve isotactic PLA from *rac*-LA, for applications requiring enhanced thermal and mechanical properties, prompted the development of a wide range of organocatalysts and metal complexes for the controlled and stereoselective ROP of lactide.^{2,7,9–11} Indeed, many studies have shown that the PLA microstructure can be controlled by the judicious choice of metal centre and ligand(s). However, despite much effort, including some computational studies,^{12–15} challenges still remain to fully understand the interplay between metal, ligand, monomer and the growing polymer chain. There remains a high degree of serendipity in the stereochemical outcome of the polymerisation, with unpredictable tacticities achieved from metal–ligand combinations.

It is noteworthy that while subtle changes in ligands have been extensively shown to induce a change in stereoselectivity,^{16–20} systematic studies across a range of metals (period or series) are less common. Several examples have however shown that the metal can significantly influence

^aDepartment of Chemistry, University of Bath, Claverton Down, Bath BA2 7AY, UK. E-mail: a.buchard@bath.ac.uk, mj205@bath.ac.uk; Tel: +44 (0)1225 386122

^bChemical Characterisation and Analysis Facility (CCAF), University of Bath, UK

†Electronic supplementary information (ESI) available: ^1H and $^{13}\text{C}\{^1\text{H}\}$ NMR spectra of $[\text{L}^{\text{Me}}\text{Sm}(\text{OiPr})_2]$ and $[\text{L}^{\text{Me}}\text{Sm}(\text{OH})_2]$; single-crystal X-ray diffraction data of all complexes; polymerisation kinetic data; DOSY NMR data; plots of M_n and D vs. conversion; SEC traces and MALDI-ToF mass spectra of polymers. CCDC 1844088–1844094. For ESI and crystallographic data in CIF or other electronic format see DOI: 10.1039/c8dt02108b

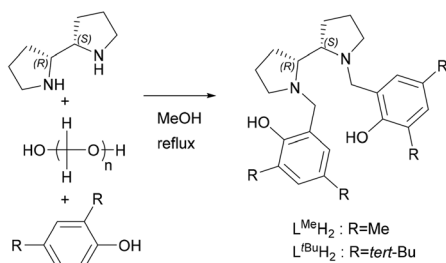
the outcome of the polymerisation.^{21,22} Changes in selectivity have thus been observed by Williams and co-workers for phosphasalen lanthanide complexes (going from heteroselective to isoselective when going from La to Lu),²³ and by Ma and co-workers for a series of aminophenolate Zn(II)/Mg(II) complexes (from heteroselectivity with Zn to isoselectivity with Mg).²⁴ We have ourselves demonstrated that a bipyrrrolidine salan ligand $L^{Me}H_2$ can lead to isotactic PLA when coordinated to Zr and Hf, atactic PLA with Ti and heterotactic PLA with Al.^{25,26} Increasing the steric bulk with $L^{tBu}H_2$ removed any selectivity when complexed to Al, but heterotactic PLA was seen with In.²⁷

Herein, we report the synthesis of a series of lanthanide (Nd, Sm, Yb) alkoxide complexes bearing these bipyrrrolidine salan ligands, their characterisation and their activity in the polymerisation of *rac*-LA. While no change in stereoselectivity was observed and synthetic challenges limited the extent of our study, we have used 1H diffusion ordered NMR spectroscopy (1H DOSY NMR) to monitor the polymer growth from the metal centres *in situ*, which also revealed a dinuclear active species.

Results and discussion

Complex synthesis

Salan ligands $L^{Me}H_2$ and $L^{tBu}H_2$ were synthesised from *meso*-2,2'-bipyrrrolidine *via* the Mannich reaction, as previously reported.²⁵ $L^{Me}H_2$ and $L^{tBu}H_2$ feature methyl and *tert*-butyl substituents at the 2- and 4-positions of the phenol rings,



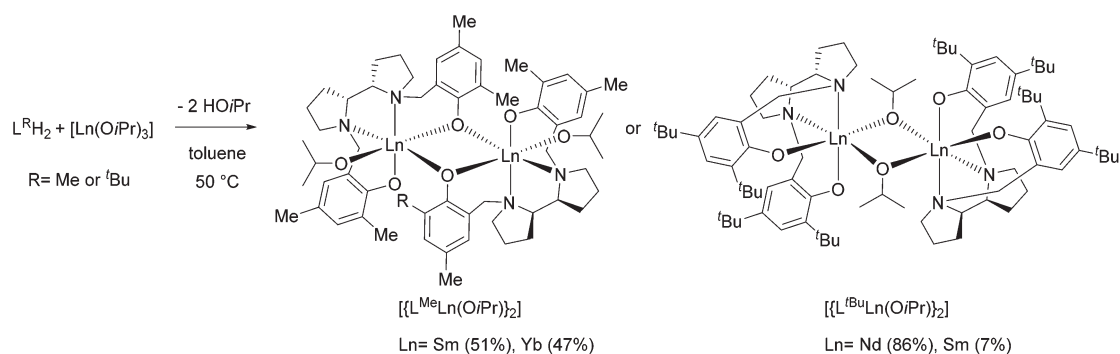
Scheme 1 Synthesis of *meso* ligands $L^{Me}H_2$ and $L^{tBu}H_2$.

respectively (Scheme 1). Metal coordination was then achieved by the reaction of the ligands with commercial lanthanide isopropoxide precursors ($[Ln(OiPr)_3]$, Ln: Nd, Sm, Yb), in anhydrous toluene at 50 °C for 3 hours, under an Ar atmosphere (see the Experimental section for details). While all possible ligand/metal combinations were attempted, only $[L^{Me}Yb(OiPr)_2]$, $[L^{Me}Sm(OiPr)_2]$, $[L^{tBu}Sm(OiPr)_2]$, and $[L^{tBu}Nd(OiPr)_2]$ dialkoxide species could be isolated as crystals, with poor to very good yields (47, 51, 7 and 86% yield, respectively).

These complexes were all characterised by elemental analysis and single crystal X-ray diffraction which are in agreement with the expected products (Scheme 2). Despite its paramagnetism, $[L^{Me}Sm(OiPr)_2]$ could also be characterised by 1H NMR (Fig. S1†). Anisotropic shifting proved more severe for Nd and Yb systems, yielding significant line broadening, a large increase in spectral width and a lower signal-to-noise ratio.²⁸ Nevertheless, some clarity was seen for $[L^{Me}Yb(OiPr)_2]$, aiding identification in the solution state and assisting during hydrolytic degradation studies (Fig. S8† and *vide infra*).

X-ray diffraction analysis revealed the influence of the ligand on the coordination pattern of the metals (Scheme 2, Fig. 1). All complexes proved to be dimeric in the solid state, with centrosymmetric structures containing two Ln centres connected to each other by two bridging μ -O atoms, and the centre of inversion sitting in the middle of the Ln_2O_2 quadrangle. However, the methyl-substituted ligand favoured the bridging of the metals by the phenoxide moiety of the ligand, whereas the *tert*-butyl-substituted ligand led to bridging isopropoxide moieties, contrasting with a *tert*-butyl tripodal bisphenolate Sm system published by Mountford and co-workers.¹³ Fig. 1 illustrates the molecular structure of representative complexes $[L^{Me}Yb(OiPr)_2]$ and $[L^{tBu}Nd(OiPr)_2]$, the Sm complexes being their isometric counterparts.

Table 1 contains selected bond lengths (Å) and angles (°) for the synthesised complexes, obtained from the X-ray diffraction analysis. Each hexacoordinated Ln atom exhibits a distorted octahedral geometry (for example, for $[L^{tBu}Nd(OiPr)_2]$, O1–Nd1–O2 = 96.35(15)°, O1–Nd1–N1 = 75.43(15)°, N2–Nd1–O3 = 166.98(14) and O2–Nd1–N2 = 72.58(15)°, with a β -*cis* conformation of the tetradentate (ONNO) ligand for all complexes, *i.e.* three atoms (O, N and N) occupying equatorial positions



Scheme 2 Synthesis of complexes $[L^{Me}Ln(OiPr)_2]$ and $[L^{tBu}Ln(OiPr)_2]$.



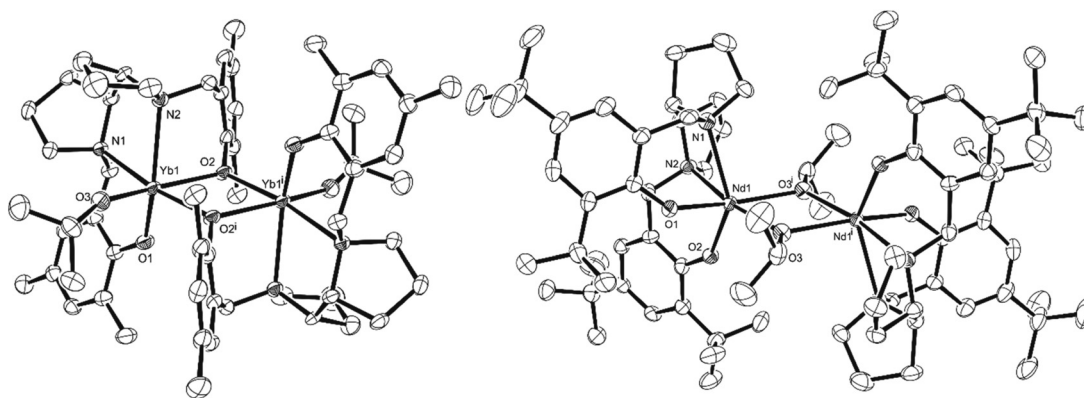


Fig. 1 ORTEP-plots (50% thermal ellipsoids) of the molecular structure of complexes $[\text{L}^{\text{Me}}\text{Yb}(\text{OiPr})]_2$ (left) and $[\text{L}^{\text{tBu}}\text{Nd}(\text{OiPr})]_2$ (right). Hydrogen atoms and residual crystallisation solvent molecules have been omitted for clarity.

Table 1 Selected bond lengths (Å) and angles (°) for solid state structures of complexes $[\text{L}^{\text{Me}}\text{Y}(\text{OiPr})]_2$, $[\text{L}^{\text{Me}}\text{Sm}(\text{OiPr})]_2$, $[\text{L}^{\text{tBu}}\text{Sm}(\text{OiPr})]_2$ and $[\text{L}^{\text{tBu}}\text{Nd}(\text{OiPr})]_2$, obtained by single crystal X-ray diffraction analysis

	$[\text{L}^{\text{Me}}\text{Yb}(\text{OiPr})]_2$	$[\text{L}^{\text{Me}}\text{Sm}(\text{OiPr})]_2$	$[\text{L}^{\text{tBu}}\text{Sm}(\text{OiPr})]_2$	$[\text{L}^{\text{tBu}}\text{Nd}(\text{OiPr})]_2$
Ln1–Ln1 ⁱ	3.6959(4)	3.8599(2)	3.8556(3)	3.8860(6)
Ln1–O1	2.112(3)	2.1902(15)	2.226(2)	2.263(4)
Ln1–O2	2.275(3)	2.3310(14)	2.177(2)	2.179(4)
Ln1–O3	2.035(3)	2.1148(16)	2.340(2)	2.336(4)
Ln1–O _{bridging} ⁱ	2.254(3)	2.3989(14)	2.342(2)	2.375(4)
Ln1–N1	2.499(4)	2.6095(16)	2.649(3)	2.580(5)
Ln1–N2	2.533(4)	2.6299(16)	2.674(3)	2.765(5)
Ln1–O _{bridging} –Ln1 ⁱ	109.39(11) (O _{bridging} = O2)	109.38(5) (O _{bridging} = O2)	110.85(10) (O _{bridging} = O3)	111.14(15) (O _{bridging} = O3)
O1–Ln1–O2	101.80(12)	102.26(5)	100.27(10)	96.35(15)
O1–Ln1–O3	103.72(14)	105.56(6)	87.95(9)	94.42(14)
O1–Ln1–N1	80.73(12)	78.81(5)	76.11(9)	75.43(15)
O1–Ln1–N2	146.76(12)	141.50(6)	91.98(9)	98.44(15)
N1–Ln1–O2	171.02(11)	168.89(5)	141.27(9)	137.54(15)

whereas one O atom is in the axial position. This is analogous to the group 4 complexes previously published.^{25,26} With these geometric features and coordination patterns in mind, it is possible that in the case of Nd, the increased ionic radius compared to Sm (1.109 Å vs. 1.079 Å) prevents the formation of $[\text{L}^{\text{Me}}\text{Nd}(\text{OiPr})]_2$, while in the case of Yb, the decreased ionic radius compared to Sm (0.985 Å vs. 1.079 Å) impedes the formation of $[\text{L}^{\text{tBu}}\text{Yb}(\text{OiPr})]_2$.

Ln–ONNO–salan–alkoxides are rare in the literature,²⁹ and to the best of our knowledge the examples reported herein represent the first Ln–salan isopropoxide species crystallographically characterised. This is surprising given the commercial availability of the tris(isopropoxide) lanthanide precursors. It is fair to say that the preferred method in the literature for Ln-mediated ROP is to prepare the lanthanide–silylamido complex, as a direct initiator or as a precursor for an alkoxide, formed by the addition of an exogenous alcohol.^{30–34}

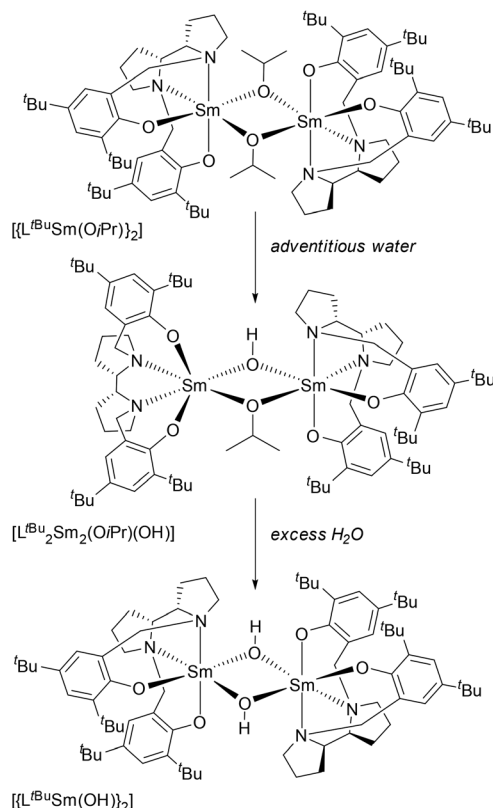
Complex hydrolytic degradation

Recently, Mehrkhodavandi and co-workers showed how a dimeric indium hydroxide species obtained from hydrolytic degradation could be returned into an active initiator for the

ROP of LA from the addition of excess alcohol.³⁵ Despite the hydrolysis products commonly reported for lanthanide alkoxide complexes, few studies actually isolate and identify such compounds with no examples reported in the context of ROP catalysis. With the potential to gain valuable insight into the degradation mechanism and role of the initiating group in the ROP of lactide, we investigated the hydrolytic degradation of our Ln–OiPr systems.

All the synthesised complexes were highly air and moisture sensitive and had to be manipulated under an inert atmosphere, using dry solvents. In fact, in the case of $[\text{L}^{\text{tBu}}\text{Sm}(\text{OiPr})]_2$, the desired complex could only be isolated with 7% crystalline yield. From the same solution of $[\text{L}^{\text{tBu}}\text{Sm}(\text{OiPr})]_2$, a second recrystallisation provided 69% yield of mono-hydroxide species $[\text{L}^{\text{tBu}}_2\text{Sm}_2(\text{OiPr})(\text{OH})]$, which was characterised by X-ray diffraction and elemental analysis, and is likely formed from adventitious moisture. Similarly, isometric $[\text{L}^{\text{tBu}}_2\text{Yb}_2(\text{OiPr})(\text{OH})]$ could also be isolated (see the ESI† for X-ray diffraction, and the Experimental section for elemental analysis data and ¹H NMR spectra). Further hydrolysis of $[\text{L}^{\text{tBu}}_2\text{Sm}_2(\text{OiPr})(\text{OH})]$ could be carried out by the addition of 10 equivalents of water, resulting in the isolation of bis-hydroxide dimer $[\text{L}^{\text{tBu}}\text{Sm}(\text{OH})]_2$, which





Scheme 3 Hydrolytic degradation of $[\{L^{tBu}Sm(OiPr)\}_2]$.

was characterised by X-ray diffraction and elemental analysis (Scheme 3). Fig. 2 presents the molecular structure of Sm complexes $[L^{tBu}_2Sm_2(OiPr)(OH)_2]$ and $[\{L^{tBu}Sm(OH)\}_2]$. Table 2 shows some key geometrical parameters of both Sm complexes. While $[\{L^{tBu}Sm(OH)\}_2]$ shows a centrosymmetric dinuclear structure with the two Sm centres bridged by the O atoms of the hydroxide groups, $[L^{tBu}_2Sm_2(OiPr)(OH)]$ features no such symmetry.

Table 2 Selected bond lengths (Å) and angles (°) for solid state structures of complexes $[L^{tBu}_2Sm_2(OiPr)(OH)]$ and $[\{L^{tBu}Sm(OH)\}_2]$, obtained by single crystal X-ray diffraction analysis

$[L^{tBu}_2Sm_2(OiPr)(OH)]$		$[\{L^{tBu}Sm(OH)\}_2]$	
Sm1–Sm2	3.8093(2)	Sm1–Sm1 ⁱ	3.8731(2)
Sm1–O1	2.1842(16)	Sm1–O1	2.1852(19)
Sm1–O2	2.1829(17)	Sm1–O2	2.2331(18)
Sm1–O3	2.3189(18)	Sm1–O3	2.1148(16)
Sm1–O4	2.3568(18)	Sm1–O3 ⁱ	2.3068(19)
Sm1–N1	2.639(2)	Sm1–N1	2.606(2)
Sm1–N2	2.633(2)	Sm1–N2	2.621(2)
Sm2–O5	2.1665(17)	Sm1–O3–Sm1 ⁱ	112.18(8)
Sm2–O6	2.2063(18)	O1–Sm1–O2	95.34(7)
Sm2–N3	2.659(2)	O1–Sm1–O3	98.30(7)
Sm2–N4	2.584(2)	O1–Sm1–N1	75.54(7)
Sm2–O3	2.2971(17)	O1–Sm1–N2	140.05(7)
Sm2–O4	2.3930(19)	N1–Sm1–O2	103.22(7)
Sm1–O3–Sm2	111.23(7)	N1–O3–O2–Ln	11.68
Sm1–O4–Sm2	106.64(8)		

In the case of methyl-substituted ligands, no crystalline products from hydrolytic degradation could be isolated. However, the hydrolysis of a solution of $[\{L^{Me}Sm(OiPr)\}_2]$ in air could be followed by ¹H NMR, which showed the progressive formation of isopropanol and of –OH groups, with no further evolution after 36 hours (Fig. S3 and 4†). DOSY NMR spectroscopy also revealed degradation product(s) to have similar metal complexes of similar size. Collectively, these elements point towards the formation of $[L^{Me}_2Sm_2(OiPr)_x(OH)_{2-x}]$ species. It is worth noting that the nature of the metal also influences hydrolysis as for $[\{L^{Me}Yb(OiPr)\}_2]$, and complete degradation with the release of a free protonated ligand was observed after *ca.* 5 hours (Fig. S9†).

Complex reactivity with lactide: monitoring by DOSY NMR

Despite their performances in the ROP of cyclic esters, in particular lactide, there are limited reactivity and mechanistic

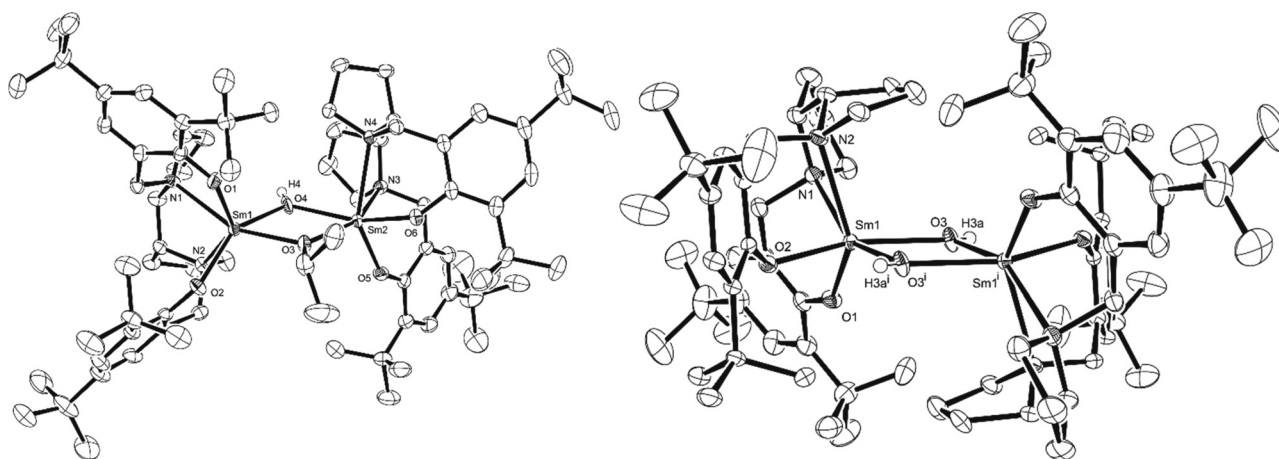


Fig. 2 ORTEP-plots (50% thermal ellipsoids) of complexes $[L^{tBu}_2Sm_2(OiPr)(OH)]$ (left) and $[\{L^{tBu}Sm(OH)\}_2]$ (right). Hydrogen atoms, except those bound to O3/O3ⁱ and residual crystallisation solvent molecules have been omitted for clarity.



studies in the literature between lanthanide complexes and lactide, as paramagnetism and fast rates make traditional methods unsuitable.³¹ However, such studies have the potential to unravel structure/activity relationships that can guide future catalyst development. Only mild isotropic shifting in the ^1H NMR of $[\{\text{L}^{\text{Me}}\text{Sm}(\text{OiPr})\}_2]$ offered the opportunity to study the fundamental reaction of the complex with lactide. While our studies did not isolate any Sm–lactide adduct or a metal complex with a growing lactide chain, we were able to achieve some insight into the reaction using Diffusion Ordered Spectroscopy (DOSY) NMR (see details in the ESI†). Recently, DOSY has become a powerful tool in polymer science, with new methodologies being developed to accurately estimate the molecular weights for macromolecules.^{36–38}

The reaction of $[\{\text{L}^{\text{Me}}\text{Sm}(\text{OiPr})\}_2]$ with 2 equivalents of *rac*-lactide (one per metal) was monitored by ^1H DOSY NMR at 25 °C in CDCl_3 in an attempt to mimic ROP conditions whilst limiting convection issues from high temperature diffusion measurements.³⁹ The dimeric structure of the complex was shown to be retained, with only a slight decrease in diffusion coefficient (Table 3, entry 2 vs. entry 1). Furthermore, this main species combined the signals of coordinated ligand L^{Me} , metal-bound isopropoxide, lactide, and an isopropyl lactate species (Fig. S11†).^{40,41} This suggests a Sm dimer species, with a lactate chain growing from one metal centre, and a lactide coordinated to a metal centre (same metal or different). This is also supported by the evaluation of the molecular weight of this species, using the method derived by Morris and co-workers (Table 3, entry 2).^{42,43}

By increasing the amount of lactide to 20 equivalents, further polymerisation could be monitored by DOSY (Fig. 3), with no evidence of any changes in the active species. The molecular weight derived by diffusion coefficients was furthermore aligned with the expected one (Table 3, entry 3). Exposing the reaction mixture to air to quench the polymerisation led to an increase in the diffusion coefficient of the polymer resonances, consistent with the cleavage of the growing polymer chain(s) from the dimer (Table 3, entry 4). The polymer was next isolated and analysed by SEC, giving M_n values consistent with those determined *via* DOSY (Fig. S26†), and giving a clear indication of only one polymer chain growing from the dimer.

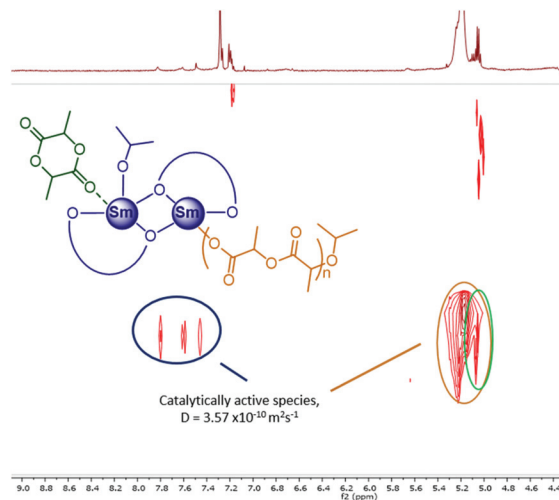


Fig. 3 ^1H DOSY NMR spectrum of the reaction between $[\{\text{L}^{\text{Me}}\text{Sm}(\text{OiPr})\}_2]$ (0.24 mmol L^{-1}) and *rac*-LA (20 equivalents, 4.8 mmol L^{-1}), 25 °C, 5 hours, CDCl_3 (1 mL) (corresponding to Table 3, entry 4).

Based on these observations, under these conditions, the catalytic active species are dinuclear, and more work is needed to establish if the presence of a second metal is advantageous or not. A cooperative mechanism could open the way to more efficient heterodinuclear metal complexes based on this ligand framework. Such an effect has been previously predicted by DFT calculations and then observed experimentally in the related ring-opening copolymerisation of epoxides and CO_2 .^{44,45}

Complex activity in the polymerisation of lactide

Complexes $[\{\text{L}^{\text{Me}}\text{Sm}(\text{OiPr})\}_2]$, $[\{\text{L}^{\text{Me}}\text{Yb}(\text{OiPr})\}_2]$ and $[\{\text{L}^{\text{tBu}}\text{Nd}(\text{OiPr})\}_2]$ were tested for the ROP of *rac*-LA under various conditions, both in solution and in the melted monomer (Table 4).

In CH_2Cl_2 at 25 °C (Table 4, entries 1–4), poor to good activity was observed, with a slight heterotactic preference, regardless of the coordination motif (P_r 0.5–0.6). Terminal alkoxide complexes $[\{\text{L}^{\text{Me}}\text{Sm}(\text{OiPr})\}_2]$ and $[\{\text{L}^{\text{Me}}\text{Yb}(\text{OiPr})\}_2]$ showed significantly lower activity than the bridging alkoxide complex $[\{\text{L}^{\text{tBu}}\text{Nd}(\text{OiPr})\}_2]$. In agreement with the insight provided by

Table 3 Reactivity of $[\{\text{L}^{\text{Me}}\text{Sm}(\text{OiPr})\}_2]$ with *rac*-LA, followed by DOSY NMR spectroscopy^a

Entry	<i>rac</i> -LA equiv.	$D, ^e 10^{-9} \text{ m}^2 \text{ s}^{-1}$	$D_{\text{solvent}}, ^e 10^{-9} \text{ m}^2 \text{ s}^{-1}$	DOSY $M_n, ^f \text{ g mol}^{-1}$	Theo. $M_n, ^g \text{ g mol}^{-1}$	SEC, $M_n, ^i \text{ g mol}^{-1}$
1	—	0.589	1.77	1269	1236	—
2 ^b	2	0.569	1.93	1371	1380	—
3 ^c	20	0.357	1.99	4091	3830	—
4 ^{c,d}	20	0.427	1.97	2668	2584 ^h	2800

^a ^1H NMR diffusion ordered spectroscopy (DOSY) studies of $[\{\text{L}^{\text{Me}}\text{Sm}(\text{OiPr})\}_2]$ in CDCl_3 (1 mL), $[\text{I}] = 2.4 \text{ mmol L}^{-1}$. ^b $[\text{I}] = 2.4 \text{ mmol L}^{-1}$, $[\text{rac-LA}] = 4.8 \text{ mmol L}^{-1}$, reaction left at 25 °C for 5 hours under Ar. ^c $[\text{I}] = 0.24 \text{ mmol L}^{-1}$, $[\text{rac-LA}] = 4.8 \text{ mM}$, reaction left at 25 °C for 24 hours under Ar. ^d After 24 h at 25 °C, the reaction was quenched by bubbling air through the system and the sample was analysed. ^e Diffusion constants taken from the middle of the contour plot mapped using a peak heights fit method. ^f Estimated from the calculated hydrodynamic radii of the diffusing species.^{42,43} ^g Calculated as: $[\text{rac-LA}]_0/[\text{I}]_0 \times M_r(\text{LA}) \times \text{conversion}/100 + M_r(\text{I})$, where $M_r(\text{I}) = 1236.5 \text{ g mol}^{-1}$ and the conversion is taken from the integration of the methine region of the ^1H NMR spectrum (*rac*-LA, $\delta = 4.98\text{--}5.08 \text{ ppm}$; PLA, $\delta = 5.09\text{--}5.24 \text{ ppm}$). ^h Calculated considering $M_r(\text{I}) = M_r(\text{HOiPr})$. ⁱ Determined by SEC in THF using triple detection methods.



Table 4 Selected polymerisation data for the polymerisation of *rac*-lactide with bis-alkoxide Ln complexes^a

Entry	Solvent	Temp. (°C)	Initiator (I)	[<i>rac</i> -LA] ₀ : [Ln]	Time (min)	Conversion ^b (%)	Theo. <i>M</i> _n ^c kg mol ⁻¹	SEC <i>M</i> _n ^d kg mol ⁻¹	<i>D</i> ^d
1	Dichloromethane	25	[^t BuNd(OiPr) ₂]	500	60	96	68.5	117.2	1.38
2	Dichloromethane	25	[^t BuNd(OiPr) ₂]	1000	60	95	136.9	247.2	1.05
3	Dichloromethane	25	[^t BuSm(OiPr) ₂]	150	120	40	8.7	5.8	1.03
4	Dichloromethane	25	[^t BuYb(OiPr) ₂]	150	120	4	—	—	—
5	Toluene	80	[^t BuNd(OiPr) ₂]	500	5	96	68.5	208.3	1.36
6	Toluene	80	[^t BuNd(OiPr) ₂]	1500	5	95	205.3	156.3	1.30
7	Toluene	80	[^t BuNd(OiPr) ₂]	3000	5	96	410.5	370.8	1.10
8	Toluene	80	[^t BuSm(OiPr) ₂]	500	5	96	69.1	350.0	1.36
9	Toluene	80	[^t BuSm(OiPr) ₂]	1500	10	96	207.4	169.4	1.23
10	Toluene	80	[^t BuYb(OiPr) ₂]	1500	10	80	173.0	101.3	1.07
11 ^e	—	130	[^t BuNd(OiPr) ₂]	900	5	95	123.1	122.1	1.05
12 ^e	—	130	[^t BuSm(OiPr) ₂]	900	5	74	96.0	136.4	1.45
13 ^e	—	130	[^t BuYb(OiPr) ₂]	900	5	91	118.1	128.8	1.24

^a For polymerisation reactions in solvent, [*rac*-LA]₀ = 0.69 mol L⁻¹. ^b Conversion is taken from the integration of the methine region of the ¹H NMR spectrum of aliquots of the crude reaction mixture (*rac*-LA, δ = 4.98–5.08 ppm; PLA, δ = 5.09–5.24 ppm). ^c Calculated as: ([*rac*-LA]₀/[Ln] × *M*_r(*rac*-LA) × conversion/100) + *M*_r(OⁱPr + H). ^d Determined by SEC in THF using triple detection methods; *D* = *M*_w/*M*_n. ^e Carried out under melt conditions using molten lactide as the solvent.

DOSY NMR, molecular weights obtained are double compared to those expected if both alkoxides were initiating polymerisation, indicative of only one polymer chain growing from the dimer. The kinetics of ROP using [^tBuNd(OiPr)₂] were investigated (Fig. S13†) and showed a pseudo-first order behaviour in monomer concentration, with *k*_{obs} of 1.7 × 10⁻³ s⁻¹ (CDCl₃, 25 °C, [LA] = 0.69 mol L⁻¹, [*rac*-LA]₀ : [Nd] = 150). For reference some of the most active systems at 25 °C from the literature include an yttrium phosphasalen based initiator developed by Williams and coworkers, which has a *k*_{obs} of 8.0 × 10⁻² s⁻¹ (THF, 25 °C, [LA] = 1 mol L⁻¹, [*rac*-LA]₀ : [Y] = 1000).^{46,47}

In toluene at 80 °C (Table 4, entries 5–10), all complexes were extremely active, achieving near quantitative conversions between 5–10 minutes for [*rac*-LA]₀ : [Ln] ratio superior to 500. Generally, bridging isopropoxide complex [^tBuNd(OiPr)₂] displayed a better control of molecular weight than bridging phenoxide ligand complexes [^tBuLn(OiPr)₂] (Ln = Sm, Yb). [^tBuNd(OiPr)₂] exhibited remarkable activity and control. In particular, when used at 166 ppm level ([*rac*-LA]₀ : [Ln] of 3000, see Table 4 entry 7), polymers with *M*_n 370 000 g mol⁻¹ and dispersity (*D*) of 1.10 could be obtained. The linear relationship between *rac*-LA conversion and *M*_n at [*rac*-LA]₀ : [Ln] of 1500 (Fig. S18†) was indicative of a well-controlled polymerisation, despite a steady increase in dispersities (*D*, reaching 1.41 after 10 min, likely due to the undesired transesterifications). Beyond this, *D* did not drastically increase even after stirring for further 30 minutes, suggesting catalyst deactivation. The kinetics of ROP using [^tBuNd(OiPr)₂] were also investigated at [*rac*-LA]₀ : [Ln] of 1500 (Fig. S16†) and showed a pseudo-first order behaviour in monomer concentration, with *k*_{obs} of 7.5 × 10⁻³ s⁻¹, a rate which is faster than the bis(phenolate) N-heterocyclic carbene Nd/Li system developed by Ni *et al.* (*k*_{obs} = 1.21 × 10⁻³ s⁻¹), tested under analogous conditions (toluene, 70 °C, [L-LA] = 1 mol L⁻¹, [L-LA]₀ : [Nd] = 1000).⁴⁸ Unfortunately, for all complexes, no tacticity bias could be observed under these conditions (*P*_r = 0.5).

No significant trend in terms of rate could be identified across the different lanthanides either. It is worth noting that SEC *M*_n values are in agreement with those expected based on the [*rac*-LA]₀ : [Ln] ratio, so that at 80 °C in toluene, every isopropoxide group of [^tBuLn(OiPr)₂] likely initiates polymerisation. Attempts to follow the polymerisation at 80 °C in toluene-d₈ by DOSY proved difficult so that further mechanistic consideration would be speculative.

Whilst not common within the rare-earth field, polymerisation reactions under industrially relevant conditions of the monomer melt at 130 °C were carried out (Table 4, entries 11–13).^{49,50} The gel point was achieved for all complexes within 5 minutes, which, in some cases hindered conversion due to mass-transfer limitations. Despite this, experimental molecular weights showed a good fit to the calculated values, assuming that all isopropoxide groups initiated polymerisation, with especially good control for [^tBuNd(OiPr)₂] (*M*_n 122 000 g mol⁻¹, *D* 1.05).

The products of hydrolytic degradation, [^tBu₂Sm₂(OiPr)(OH)] and [^tBu₂Yb₂(OiPr)(OH)], were also tested in the ROP of *rac*-LA and showed comparable activity to bis-alkoxide species, albeit with less control (see ESI, Tables S1–S3†). This is likely due to the –OH group being a slow polymerisation initiator, in addition to leading to carboxylic-acid terminated polymer chains, which could act as chain termination or chain transfer agents.

Conclusion

In conclusion, four new dimeric lanthanide alkoxide complexes with bipyrrrolidine salan ligands have been prepared, and complexes have been characterised *via* single-crystal X-ray diffraction and elemental analysis. Various coordination motifs were seen depending on the ligand and the metal used. The hydrolytic degradation of these complexes allowed the preparation of three dimeric mixed alkoxide/hydroxide and



bis-hydroxide products. $[\{L^{tBu}Nd(OiPr)\}_2]$ proved to be very active for the controlled ring-opening polymerisation (ROP) of *rac*-lactide (LA), in melt monomer and in solution, yielding a high molecular weight polymer (up to $370\,000\text{ g mol}^{-1}$) in a predictable and controlled fashion. In particular, under industrially relevant conditions ($130\text{ }^\circ\text{C}$ in melt monomer), PLA with $M_n\ 122\,000\text{ g mol}^{-1}$ ($D\ 1.05$) could be achieved in 5 minutes. ^1H DOSY NMR spectroscopy was employed to investigate the nature of the catalytic active species, which proved to be dinuclear.

Experimental section

Materials and methods

All metal complexes were synthesised under anhydrous conditions, using MBraun gloveboxes and standard Schlenk techniques. All chemicals used were purchased from Strem and Sigma-Aldrich and used as received unless stated otherwise. Dry solvents were obtained from an MBraun solvent purification system and stored under nitrogen over 3 \AA molecular sieves. CDCl_3 was dried over CaH_2 , distilled prior to use, and stored under nitrogen. *rac*-LA was recrystallised twice from dry toluene and stored under nitrogen. Ligands L^{Me} and L^{tBu} were synthesised following the literature procedures.²⁵ NMR spectra were recorded using a Bruker Avance III 500 MHz spectrometer. Coupling constants are given in hertz. DOSY NMR experiments were carried out at a concentration of 10 mg mL^{-1} of monomer in 1 mL deuterated CDCl_3 (see details in the ESI†) and processed using MestReNova software (v10). Diffusion coefficients were determined by comparing against solvent diffusion signals and comparing with those recorded in the literature.⁴³ Elemental analysis was determined by Stephen Boyer at London Metropolitan University. SEC was performed using two PL MIXED.D $300 \times 7.5\text{ mm}$ columns in series, with THF as the eluent, at a flow rate of 1 mL min^{-1} on an Agilent 1260 GPC/SEC MDS instrument at $35\text{ }^\circ\text{C}$. The polymer samples were dissolved in SEC grade THF and filtered prior to analysis. Molecular weights were determined using triple detection methods (differential refractive index detector (calibrated using polystyrene standards), a viscometer detector and a light scattering detector (90° , with a calculated dn/dc range = $0.095\text{--}0.11\text{ mL g}^{-1}$, as calculated from the RI)). MALDI-ToF spectrometry analysis was carried out on a Bruker Autoflex speed instrument in the reflector positive mode, using DCTB (*trans*-2-[3-(4-*tert*-butylphenyl)-2-methyl-2-propenylidene] malononitrile) as the matrix at a concentration of 10 mg mL^{-1} in THF, with added sodium trifluoroacetate (see the ESI†). All X-ray diffraction data were obtained at 150 K , on a Rigaku SuperNova or Excalibur diffractometer using $\text{Cu-K}\alpha$ or $\text{Mo-K}\alpha$ radiation ($\lambda = 1.54184\text{ \AA}$ or 0.71073 \AA). Structures were solved using the SHELXL-2014 suite of programs.

Complex synthetic procedure

In a typical experiment, ligand L^{tBu} (576 mg , 1.0 mmol), was dissolved in toluene (5 mL) then added to a stirred solution of

$[\text{Nd}(\text{OiPr})_3](1.0\text{ mmol})$ in toluene (10 mL). The solution was then heated to $60\text{ }^\circ\text{C}$ and left to stir for 3 hours. After this time the solvent was removed and the solid was dissolved in the minimum quantity of dry hexane/toluene and recrystallised at $-20\text{ }^\circ\text{C}$. The resulting crystalline solid was washed with cold dry hexane ($3 \times 1\text{ mL}$) and then dried, to yield the product as a solid, and stored under an argon atmosphere.

$[\{L^{tBu}Nd(\text{OiPr})\}_2]$. Blue powder (680 mg , 86% yield). Elemental (CHN) analysis; (calculated: $\text{C}_{82}\text{H}_{130}\text{N}_4\text{O}_6\text{Nd}_2$) C 63.2% , H: 8.42% , N: 3.60% , (experimental) C: 62.74% , H: 8.16% , N: 3.62% .

$[\{L^{tBu}Sm(\text{OiPr})\}_2]$. White powder (55 mg , 7% yield). Elemental (CHN) analysis; (calculated: $\text{C}_{82}\text{H}_{130}\text{N}_4\text{O}_6\text{Sm}_2$) C: 62.79% , H: 8.35% , N: 3.57% , (experimental) C: 63.41% , H: 8.79% , N: 3.61% .

$[\{L^{\text{Me}}Sm(\text{OiPr})\}_2]$. White powder (310 mg , 51% yield). ^1H NMR (500 MHz , CDCl_3 , δ_{H} , ppm); 7.92 (2H, ArH), 7.43 (2H, ArH), 6.90 (2H, ArH), 6.25 (2H, d, $J = 12.5\text{ Hz}$, CHH), 6.18 (2H, OCH(CH_3)₂), 6.01 (6H, CH_3), 5.21 (2H, CHH), 4.8 (2H, ArH), 2.83 (2H, d, $J = 12.5\text{ Hz}$, CHH), 2.50 (6H, CH_3), $2.05\text{--}2.32$ (12H, OCH(CH_3)₂), 2.00 (6H, CH_3), 1.88 (2H, CHH), 0.72 (4H, CH_2), 0.2 (6H, CH_3), -0.04 (2H, CH), -0.33 (2H, CH), -0.33 (2H, CH), -0.69 (4H, CH_2), -1.02 (4H, CH_2), -1.53 (2H, CH), -2.45 (2H, CH), -2.70 (2H, CH), -4.07 (2H, CH), -4.56 (2H, CH). 2D DOSY (500 MHz , CDCl_3 , $D_{\text{sol}} = 1.77 \times 10^{-9}\text{ m}^2\text{ s}^{-1}$, 298 K) $5.89 \times 10^{-10}\text{ m}^2\text{ s}^{-1}$. Elemental (CHN) analysis; (calculated: $\text{C}_{58}\text{H}_{82}\text{N}_4\text{O}_6\text{Sm}_2$) C: 56.54% , H: 6.71% , N: 4.55% , (experimental) C: 56.70% , H: 6.81% , N: 4.46% .

$[\{L^{\text{Me}}Yb(\text{OiPr})\}_2]$. White powder (298 mg , 47% yield). Elemental (CHN) analysis; (calculated: $\text{C}_{58}\text{H}_{82}\text{N}_4\text{O}_6\text{Yb}_2$) C: 54.53% , H: 6.47% , N: 4.39% , (experimental) C: 54.16% , H: 6.59% , N: 4.34% .

The isolation of degradation products could be achieved from recrystallisation of the filtrate from the precipitation of the analogous bis-alkoxide complex. Washing with cold hexane ($3 \times 10\text{ mL}$) and drying under vacuum yielded a crystalline material which could be characterised by CHN analysis and single crystal X-ray diffraction. Hydrolysis reactions monitored by ^1H NMR as in the case of $[\{L^{\text{Me}}Yb(\text{OiPr})\}_2]$ and $[\{L^{\text{Me}}Sm(\text{OiPr})\}_2]$ were carried out by exposing a solution of lanthanide sample in CDCl_3 in a J-Young tube to a flow of compressed air for 30 min. The vessel was sealed and monitored via ^1H NMR spectroscopy.

$[\{L^{tBu}_2\text{Sm}_2(\text{OiPr})(\text{OH})\}]$. Cream powder (530 mg , 69% yield). Elemental (CHN) analysis; (calculated: $\text{C}_{79}\text{H}_{124}\text{N}_4\text{O}_6\text{Sm}_2$) C: 62.16% , H: 8.19% , N: 3.67% , (experimental) C: 61.66% , H: 8.15% , N: 3.68% .

$[\{L^{tBu}_2\text{Yb}_2(\text{OiPr})(\text{OH})\}]$. White powder (298 mg , 47% yield). Elemental (CHN) analysis; (calculated: $\text{C}_{79}\text{H}_{124}\text{N}_4\text{O}_6\text{Yb}_2$) C: 54.53% , H: 6.47% , N: 4.39% , (experimental) C: 54.16% , H: 6.59% , N: 4.34% .

$[\{L^{tBu}Sm(\text{OH})\}_2]$. White powder (90 mg , 18% yield). ^1H NMR (500 MHz , CDCl_3 , δ_{H} , ppm); 22.36 (1H, SmOH), 8.28 (2H, ArH), 8.05 (2H, ArH), 6.63 (2H, CHH), 3.14 (4H, NCH_2), 2.87 (2H, CHH), 1.93 (18H, ($\text{C}(\text{CH}_3)_3$)), 0.54 (18H, ($\text{C}(\text{CH}_3)_3$)), -0.85 (2H, CH_2), -2.04 (2H, CH_2), -3.02 (2H, CH_2), -4.48 (2H, CH_2),



−7.22 (2H, CH₂); ¹³C{¹H} NMR (100 MHz, CDCl₃, δ_C, ppm); 172.4 (C=O), 137.1 (Ar), 135.7 (Ar), 128.4 (Ar), 127.8 (Ar), 126.0 (Ar), 66.6 (NCH), 59.6 (NCH₂), 52.8 (NCH₂), 36.0 (C(CH₃)₃), 35.2 (C(CH₃)₃), 32.6 (C(CH₃)₃), 29.6 (C(CH₃)₃), 22.8 (CH)₂, 18.7 (CH)₂, 16.8 (CH)₂, 14.3 (CH)₂. 2D DOSY (500 MHz, CDCl₃, D_{sol} = 2.09 × 10^{−9} m² s^{−1}, 298 K) 4.69 × 10^{−10} m² s^{−1}. Elemental (CHN) analysis, (calculated: C₇₆H₁₁₈N₄O₆Sm₂) C: 61.49%, H: 8.01%, N 3.77%, (experimental) C: 60.96%, H 7.77%, N 3.74%.

Polymerisation of lactide

Polymerisation in solution. In a typical experiment, *rac*-lactide (1.0 g, 6.9 × 10^{−3} mol) was added to an ampule with a J-Young cap in 10 mL of solvent, with the initiator (6.9 × 10^{−6} mol). If toluene was the chosen solvent, the polymerisation ran at 80 °C for the chosen time, whereas polymerisations in CH₂Cl₂ were carried out at 25 °C. Once complete the solvent was immediately removed *in vacuo* and the crude product was analysed *via* ¹H NMR. The polymer was then washed with methanol (3 × 10 mL) and dried under high vacuum prior to GPC analysis.

Polymerisation in monomer melt. In a typical experiment, *rac*-lactide (1.0 g, 6.9 × 10^{−3} mol) was added to an ampule with a J-Young cap with the initiator (7.7 × 10^{−6} mol) and placed in an oil bath set at 130 °C. Upon solidification of the mixture, the vial was exposed to air and approximately 5 mL of reagent grade CH₂Cl₂ was added to terminate the polymerisation. Removal of the solvent *in vacuo* yielded the crude product which was analysed *via* ¹H NMR spectroscopy. The polymer was then washed with methanol (3 × 10 mL) and dried under high vacuum.

In situ monitoring of polymerisation kinetics. In a typical experiment, *rac*-lactide (60 mg, 4.16 × 10^{−4} mol) was added to an NMR tube with a J-Young cap in 0.6 mL of tol-d₈, with a metal complex initiator (1.38 × 10^{−6} mol). The tube was allowed to equilibrate at 80 °C for 5 minutes, the magnetic field was homogenised and experiments were ran for 5 minutes until completion. Quenching of the reaction was carried out by bubbling compressed air with a needle through the solvent for 5 minutes.

Conflicts of interest

There are no conflicts to declare.

Acknowledgements

We thank the EPSRC and University of Bath for funding a studentship for JB. AB acknowledges Roger and Sue Whorrod (fellowship) and the Royal Society (UF/160021 fellowship). Analytical facilities were provided through the Chemical Characterisation and Analysis Facility (CCAF) at the University of Bath (<http://www.bath.ac.uk/ccaf>).

Notes and references

- 1 R. Geyer, J. R. Jambeck and K. L. Law, *Sci. Adv.*, 2017, **3**, 5.
- 2 X. Zhang, M. Fevre, G. O. Jones and R. M. Waymouth, *Chem. Rev.*, 2018, **118**, 839–885.
- 3 J. H. Song, R. J. Murphy, R. Narayan and G. B. H. Davies, *Philos. Trans. R. Soc., B*, 2009, **364**, 2127–2139.
- 4 J. C. Philp, A. Bartsev, R. J. Ritchie, M. A. Baucher and K. Guy, *New Biotechnol.*, 2013, **30**, 635–646.
- 5 N. Hernández, R. C. Williams and E. W. Cochran, *Org. Biomol. Chem.*, 2014, **12**, 2834–2849.
- 6 E. T. H. Vink, S. Davies and J. J. Kolstad, *Ind. Biotechnol.*, 2010, **6**, 212–224.
- 7 M. J. Stanford and A. P. Dove, *Chem. Soc. Rev.*, 2010, **39**, 486–494.
- 8 H. Tsuji, *Macromol. Biosci.*, 2005, **5**, 569–597.
- 9 S. Dagorne, M. Normand, E. Kirillov and J. F. Carpentier, *Coord. Chem. Rev.*, 2013, **257**, 1869–1886.
- 10 W. Zhao, C. Li, B. Liu, X. Wang, P. Li, Y. Wang, C. Wu, C. Yao, T. Tang, X. Liu and D. Cui, *Macromolecules*, 2014, **47**, 5586–5594.
- 11 A. Buchard, C. M. Bakewell, J. Weiner and C. K. Williams, *Organometallics and Renewables*, 2012, vol. 39.
- 12 A. P. Dove, V. C. Gibson, E. L. Marshall, H. S. Rzepa, A. J. P. White and D. J. Williams, *J. Am. Chem. Soc.*, 2006, **128**, 9834–9843.
- 13 H. E. Dyer, S. Huijser, N. Susperregui, F. Bonnet, A. D. Schwarz, R. Duchateau, L. Maron and P. Mountford, *Organometallics*, 2010, **29**, 3602–3621.
- 14 E. L. Marshall, V. C. Gibson and H. S. Rzepa, *J. Am. Chem. Soc.*, 2005, **127**, 6048–6051.
- 15 D. E. Stasiw, A. M. Luke, T. Rosen, A. B. League, M. Mandal, B. D. Neisen, C. J. Cramer, M. Kol and W. B. Tolman, *Inorg. Chem.*, 2017, **56**, 14366–14372.
- 16 Y. Cui, C. Chen, Y. Sun, J. Wu and X. Pan, *Inorg. Chem. Front.*, 2017, **4**, 261–269.
- 17 P. Hormnirun, E. L. Marshall, V. C. Gibson, A. J. P. White and D. J. Williams, *J. Am. Chem. Soc.*, 2004, **126**, 2688–2689.
- 18 C. Bakewell, T. P. A. Cao, N. Long, X. F. Le Goff, A. Auffrant and C. K. Williams, *J. Am. Chem. Soc.*, 2012, **134**, 20577–20580.
- 19 I. Yu, A. Acosta-Ramírez and P. Mehrkhodavandi, *J. Am. Chem. Soc.*, 2012, **134**, 12758–12773.
- 20 K. Press, I. Goldberg and M. Kol, *Angew. Chem., Int. Ed.*, 2015, **54**, 14858–14861.
- 21 J. Bhattacharjee, A. Harinath, H. P. Nayek, A. Sarkar and T. K. Panda, *Chem. – Eur. J.*, 2017, **23**, 9319–9331.
- 22 C. Bakewell, A. J. P. White, N. J. Long and C. K. Williams, *Inorg. Chem.*, 2015, **54**, 2204–2212.
- 23 C. Bakewell, A. J. P. White, N. J. Long and C. K. Williams, *Angew. Chem., Int. Ed.*, 2014, **53**, 9226–9230.
- 24 H. Wang, Y. Yang and H. Ma, *Macromolecules*, 2014, **47**, 7750–7764.
- 25 M. D. Jones, S. L. Hancock, P. McKeown, P. M. Schafer, A. Buchard, L. H. Thomas, M. F. Mahon and J. P. Lowe, *Chem. Commun.*, 2014, **50**, 15967–15970.



- 26 M. D. Jones, L. Brady, P. McKeown, A. Buchard, P. M. Schäfer, L. H. Thomas, M. F. Mahon, T. J. Woodman and J. P. Lowe, *Chem. Sci.*, 2015, **6**, 5034–5039.
- 27 J. Beament, M. F. Mahon, A. Buchard and M. D. Jones, *New J. Chem.*, 2017, **41**, 2198–2203.
- 28 W. D. Horrocks and J. P. Sipe, *J. Am. Chem. Soc.*, 1971, **93**, 6800–6804.
- 29 J. F. Carpentier, *Organometallics*, 2015, **34**, 4175–4189.
- 30 W. Li, Z. Zhang, Y. Yao, Y. Zhang and Q. Shen, *Organometallics*, 2012, **31**, 3499–3511.
- 31 X. Liu, X. Shang, T. Tang, N. Hu, F. Pei, D. Cui, X. Chen and X. Jing, *Organometallics*, 2007, **26**, 2747–2757.
- 32 Z. Zhang, X. Xu, W. Li, Y. Yao, Y. Zhang, Q. Shen and Y. Luo, *Inorg. Chem.*, 2009, **48**, 5715–5724.
- 33 T. Zeng, Q. Qian, B. Zhao, D. Yuan, Y. Yao and Q. Shen, *RSC Adv.*, 2015, **5**, 53161–53171.
- 34 F. Bonnet, A. R. Cowley and P. Mountford, *Inorg. Chem.*, 2005, **44**, 9046–9055.
- 35 T. Ebrahimi, D. C. Aluthge, B. O. Patrick, S. G. Hatzikiriakos and P. Mehrkhodavandi, *ACS Catal.*, 2017, **7**, 6413–6418.
- 36 P. Lewinski, S. Sosnowski, S. Kazmierski and S. Penczek, *Polym. Chem.*, 2015, **6**, 4353–4357.
- 37 W. Li, H. Chung, C. Daeffler, J. A. Johnson and R. H. Grubbs, *Macromolecules*, 2012, **45**, 9595–9603.
- 38 J. G. Rosenboom, J. De Roo, G. Storti and M. Morbidelli, *Macromol. Chem. Phys.*, 2017, **218**, 1–10.
- 39 I. Swan, M. Reid, P. W. A. Howe, M. A. Connell, M. Nilsson, M. A. Moore and G. A. Morris, *J. Magn. Reson.*, 2015, **252**, 120–129.
- 40 F. Isnard, M. Lamberti, L. Lettieri, I. D'auria, K. Press, R. Troiano and M. Mazzeo, *Dalton Trans.*, 2016, **45**, 16001–16010.
- 41 M. Lu, Y. Yao, Y. Zhang and Q. Shen, *Dalton Trans.*, 2010, **39**, 9530–9537.
- 42 R. Evans, G. Dal Poggetto, M. Nilsson and G. A. Morris, *Anal. Chem.*, 2018, **90**, 3987–3994.
- 43 R. Evans, Z. Deng, A. K. Rogerson, A. S. McLachlan, J. J. Richards, M. Nilsson and G. A. Morris, *Angew. Chem., Int. Ed.*, 2013, **52**, 3199–3202.
- 44 A. Buchard, F. Jutz, M. R. Kember, A. J. P. White, H. S. Rzepa and C. K. Williams, *Macromolecules*, 2012, **45**, 6781–6795.
- 45 J. A. Garden, P. K. Saini and C. K. Williams, *J. Am. Chem. Soc.*, 2015, **137**, 15078–15081.
- 46 T. P. A. Cao, A. Buchard, X. F. Le Goff, A. Auffrant and C. K. Williams, *Inorg. Chem.*, 2012, **51**, 2157–2169.
- 47 R. H. Platel, L. M. Hodgson and C. K. Williams, *Polym. Rev.*, 2008, **48**, 11–63.
- 48 M. Zhang, X. Ni and Z. Shen, *Organometallics*, 2014, **33**, 6861–6867.
- 49 F. Bonnet, F. Stoffelbach, G. Fontaine and S. Bourbigot, *RSC Adv.*, 2015, **5**, 31303–31310.
- 50 R. D. Kohn, Z. Pan, J. Sun and C. Liang, *Catal. Commun.*, 2003, **4**, 33–37.

